

We are IntechOpen, the world's leading publisher of Open Access books Built by scientists, for scientists

4,800

Open access books available

122,000

International authors and editors

135M

Downloads

Our authors are among the

154

Countries delivered to

TOP 1%

most cited scientists

12.2%

Contributors from top 500 universities



WEB OF SCIENCE™

Selection of our books indexed in the Book Citation Index
in Web of Science™ Core Collection (BKCI)

Interested in publishing with us?
Contact book.department@intechopen.com

Numbers displayed above are based on latest data collected.

For more information visit www.intechopen.com



Simulated Performance of Conical Antennas Using Matlab-Based Finite-Difference Time Domain (FDTD) Code

George S. Kliros

*Hellenic Air-Force Academy, Department of Aeronautical Sciences,
Division of Electronics and Communication Engineering
Greece*

1. Introduction

The need of ultrawideband (UWB) antennas with omni-directional coverage is increasing for both military and commercial applications (Wiesbeck *et. al.*, 2009; Minin, 2010). The UWB radio technology promises high resolution radar applications, sensor networks with a large number of sensors for industrial or home surveillance as well as high data-rate communication over short range for personal area networks. With a need for antennas with the characteristics of broad bandwidth and small electrical size, conical antenna structures have been a focus of research because of its broad bandwidth and omni-directional radiation pattern (Maloney & Smith, 1993; Sandler & King, 1994; Yu & Li, 2008; Palud *et. al.*, 2008). The bi-conical antenna exhibits a very stable omni-directional radiation pattern in the plane normal to the dipole axis together with an excellent transient response. However, the feeding with a usual coaxial cable requires a balun, which transforms the asymmetric mode of the feed line into a symmetric mode at the feed point. For the coaxial balun the ultra wide bandwidth demands very high precision in the manufacturing process in order to get a good and stable matching especially for the high frequencies. The mono-cone antenna as asymmetric structure does not need any balun for an asymmetric feed line but it needs an infinite ground plane, which in reality can only be approximated. The theory of wide-angle conical antennas has been developed sufficiently to permit calculation of the transfer functions relating source voltage to radiated field and incident field to load voltage over the range of frequencies required in the study of transients. Such calculations were demonstrated in (Harrison & Williams, 1965).

Due to their three-dimensional configurations, conical antennas are bulky and difficult to fabricate, integrate, and reconfigure. Moreover, since conventional conical antennas comprise of free-standing metal, they are typically heavy in order to achieve sufficient mechanical stability. Several configurations have been proposed to improve conical antennas' mechanical performance (Ma *et. al.*, 2009; Zhou *et. al.*, 2009, Kliros *et. al.*, 2010a). Resistive loading for conical antennas, which is investigated in (Maloney 1993), does not constitute the optimal solution as it reduces the antennas' efficiency. Recently, investigations have been carried out on configurations that employ a dielectric or magnetic material to cover the conical antenna (Gentili *et. al.*, 2004, Lu, 2007). Dielectric and magnetic coating of

the radiating cone, enables making the antenna electrically smaller and more rugged while maintaining a wide band input impedance.

In this chapter, we present a Finite Difference Time Domain (FDTD) code in spherical coordinates implemented in MATLAB in order to simulate the performance of dielectric covered conical antennas. MATLAB provides an interactive environment for algorithm development, data post-processing and visualization. The spherical FDTD equations can be found using a modified Yee cell in spherical coordinates (Fusco, 1990). Spherical Berenger's perfectly matched layer (PML) is applied as absorbing boundary condition where a parabolic conductivity profile in the spherical PML-region is used (Berenger, 1996). A unique feature of the PML is that electromagnetic waves of arbitrary incidence, polarization and frequency are matched at the boundary in a reflectionless manner. Results concerning time evolution of the radiated electromagnetic field, the return loss, input impedance, maximum gain as well as far-field radiation patterns across an extended bandwidth, are presented. A time domain study has also been performed to characterize the antenna's behaviour in case an UWB pulse is used. For evaluating waveform distortions caused by the antenna, we examine the degree of similarity between source pulse and received pulse waveforms in several propagation directions. The effect of the dielectric spherical cover on the antenna's performance is investigated. The author mostly worked in MATLAB version 7.4 and the related sample codes are provided in the Appendix.

2. Conical antenna design and analysis

In this section, we present the design of a conical antenna covered by a dielectric material with hemispherical shape and describe the FDTD algorithm in spherical coordinates for the analysis of the radiation as well as the time-domain characteristics of the antenna. Dielectric coating of the metallic radiating cone enables making the antenna electrically smaller and more rugged while maintaining a wide band input impedance. Moreover, dielectric coating enables the design of a quasi-planar structure with approximately omni-directional radiation pattern. Therefore, this antenna can be easily integrated with planar circuits.

2.1 Conical antenna geometry

The dielectric covered conical antenna is illustrated in Fig. 1 and can be described by two parameters: the half-cone angle (flare angle) θ_0 and the length of the cone's arm antenna length) ℓ . The spherical dielectric cover is made of homogeneous material with permittivity $\epsilon_r\epsilon_0$ and permeability $\mu_r\mu_0$, where ϵ_0 and μ_0 are the permittivity and permeability of free space, respectively. The addition of the dielectric cover provides mechanical support to conical radiator and enables physical size reduction of the antenna. The bottom side of the dielectric is coated by metal and behaves as the ground plane. The metallic cone and the ground plane jointly form a mono-cone radiator. The antenna is fed by a coaxial connector, with its outer and inner conductors connected to the ground plane and the cone tip respectively.

The radiation mechanism of this dielectric covered antenna is similar to the conventional mono-conical antenna (Liang & Wah, 2000). Since the feed is located at the center of a revolutionarily symmetric structure, spherical transverse electromagnetic (TEM) wave is launched in the dielectric material. When the TEM wave hits the end of the cone, it is reflected and scattered. The reflection and scattering attenuate as frequency increases and therefore, the antenna approaches a semi-infinitely long transmission line for high

frequencies. Compared to conventional mono-conical antennas, the addition of the dielectric cover introduces some complications (Lu *et. al.*, 2007):

- a. The wavelength within the dielectric material is shorter than that in the air and as a result, the electrical length of the antenna increases. This affects the UWB performance of the antenna.
- b. The dielectric-air interface results in more reflection and scattering of the outgoing TEM wave, making the antenna less matched to free space.
- c. The dielectric material forms a cavity that stores energy, hence would reduce the antenna's bandwidth.
- d. The conductivity of the dielectric cover would reduce the antenna's efficiency and low dielectric loss should be another criterion for the antenna's cover.

Consequently, it is not easy to predict the effect of the dielectric cover on the performance of the conical antenna for UWB applications.

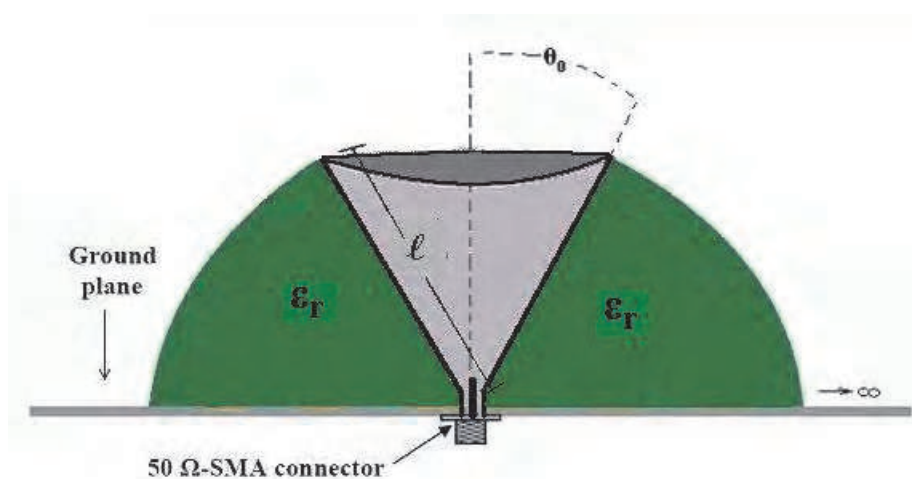


Fig. 1. Geometry of the dielectric covered conical antenna.

2.2 FDTD Method in spherical coordinates

FDTD method is very suitable for analysing and optimising the antenna for UWB radio technology. The method becomes one of the attractive methods due to its programming simplicity and flexibility in analyzing wide range of electromagnetic structures. Cartesian-grid FDTD technique utilizes a cubic prism as a unit cell. Thus, it may produce significant errors when modelling perfect electric conductors with curved surfaces and edges because of the staircase approximation introduced in the process. In this section, the FDTD algorithm in spherical coordinates is described following the lines of (Liu & Grimes, 1999; Brocato, 2004). The Maxwell's equations in finite difference form, the suitable absorbing boundary conditions and the input voltage source model are presented.

2.2.1 Spherical FDTD Equations for a conical antenna

The FDTD equations are derived directly from Maxwell's curl equations in the time domain. Taking into account the medium properties, Maxwell's curl equations can be written as:

$$\nabla \times \vec{E} = -\mu \cdot \frac{\partial \vec{H}}{\partial t} - \sigma^* \cdot \vec{H} \quad (1)$$

$$\nabla \times \vec{H} = \varepsilon \cdot \frac{\partial \vec{E}}{\partial t} + \sigma \cdot \vec{E} \quad (2)$$

where ε and μ are the permittivity and permeability respectively and, σ and σ^* the electric and magnetic conductivity of the propagation space respectively. These two vector equations are the general equations governing the antenna operation. Because the conical antenna is a revolutionary symmetric structure, the three dimensional problem can be reduced to two-dimensional problem. In spherical coordinates, due to rotational symmetry, Eq. (1) and (2) lead to the following three scalar partial differential equations:

$$\frac{\partial H_\phi}{\partial t} = -\frac{\sigma^*}{\mu} \cdot H_\phi - \frac{1}{\mu \cdot r \cdot \sin \theta} \left(\sin \theta \frac{\partial}{\partial r} (r \cdot E_\theta) - \frac{\partial}{\partial \theta} (\sin \theta \cdot E_r) \right) \quad (3)$$

$$\frac{\partial E_r}{\partial t} = -\frac{\sigma}{\varepsilon} \cdot E_r + \frac{1}{\varepsilon \cdot r \cdot \sin \theta} \frac{\partial}{\partial \theta} (\sin \theta \cdot H_\phi) \quad (4)$$

$$\frac{\partial E_\theta}{\partial t} = -\frac{\sigma}{\varepsilon} \cdot E_\theta - \frac{1}{\varepsilon \cdot r} \frac{\partial}{\partial r} (r \cdot H_\phi) \quad (5)$$

To obtain a discrete set of the continuous differential equations, the central difference approximation is used on both the time and space first-order partial derivatives. The entire computational space is a collection of modified Yee unit cells (Yee, 1966). In our modified Yee's scheme, the computational space is subdivided by using an orthogonal mesh in spherical coordinates. The electric fields are located along the edges of the cells, while the magnetic fields are positioned at the centers of these cells. Using the well-known half time step notation in all locations and after some rearrangements, a set of finite difference field forms for Eqs. (3)-(5) follows (Kliros *et. al.*, 2010a, 2010b):

$$E_r^{n+1}(i, j) = C_a(i) E_r^n(i, j) + \frac{C_b(i)}{(i+1/2)\Delta\theta} \left[\frac{\sin((j+1/2)\Delta\theta)}{\sin((j-1/2)\Delta\theta)} H_\phi^{n+\frac{1}{2}}(i, j) - H_\phi^{n+\frac{1}{2}}(i, j-1) \right] \quad (6)$$

$$E_\theta^{n+1}(i, j) = C_a(i) E_\theta^n(i, j) + C_b(i) \cdot \left[H_\phi^{n+\frac{1}{2}}(i-1, j) - \left(\frac{i+1/2}{i-1/2} \right) \cdot H_\phi^{n+\frac{1}{2}}(i, j) \right] \quad (7)$$

$$H_\phi^{n+\frac{1}{2}}(i, j) = D_a(i) H_\phi^{n-\frac{1}{2}}(i, j) + \frac{D_b(i)}{(i+1/2)\Delta\theta} \left[\frac{\sin((j+1)\Delta\theta)}{\sin(j\Delta\theta)} E_r^n(i, j+1) - E_r^n(i, j) \right] - D_b(i) \left[\left(\frac{i+1}{i} \right) E_\theta^n(i+1, j) - E_\theta^n(i, j) \right] \quad (8)$$

where

$$C_a(i) = \frac{1 - \frac{\sigma(i)\Delta t}{2\varepsilon(i)}}{1 + \frac{\sigma(i)\Delta t}{2\varepsilon(i)}}, \quad C_b(i) = \frac{\frac{\Delta t}{\varepsilon(i)\Delta r}}{1 + \frac{\sigma(i)\Delta t}{2\varepsilon(i)}} \quad (9)$$

$$D_a(i) = \frac{1 - \frac{\sigma^*(i)\Delta t}{2\mu(i)}}{1 + \frac{\sigma^*(i)\Delta t}{2\mu(i)}}, \quad D_b(i) = \frac{\frac{\Delta t}{\mu(i)\Delta r}}{1 + \frac{\sigma^*(i)\Delta t}{2\mu(i)}} \quad (10)$$

and Δr , $\Delta\theta$ represent the step size in the r - and θ - directions, respectively. Superscript n signifies that the quantities are to be evaluated at $t = n\Delta t$, and, i and j represent the point $(i\Delta r, j\Delta\theta)$ in the spherical grid. The half time steps indicate that the fields E and H are calculated alternately. The maximum time step is limited by the stability Courant's criterion (Fusco, 1990):

$$\Delta t \leq \min \frac{r(\Delta r)(\Delta\theta)}{c\sqrt{(\Delta r)^2 + (r\Delta\theta)^2}} \quad (11)$$

where c is the velocity of the light in free space.

2.2.2 Absorbing Boundary Conditions (ABC) treatment

In order to study antenna matching and pulse fidelity in the time domain, any spurious reflections had to be eliminated using suitable absorbing boundary conditions (ABC). Because we treat the problem using spherical coordinates, the absorbing boundary layer should be spherically symmetric as shown in Fig. 2. The purpose of the PML is to simulate an infinite simulation space, that is, outgoing waves are absorbed by the PML and cannot reflect back into simulation space. A unique feature of the PML is that plane waves of arbitrary incidence, polarization and frequency are matched at the boundary in a reflectionless manner. The boundary of the computational space must be sufficiently far from the antenna, usually in a distance at least ten times the free space operating wavelength.

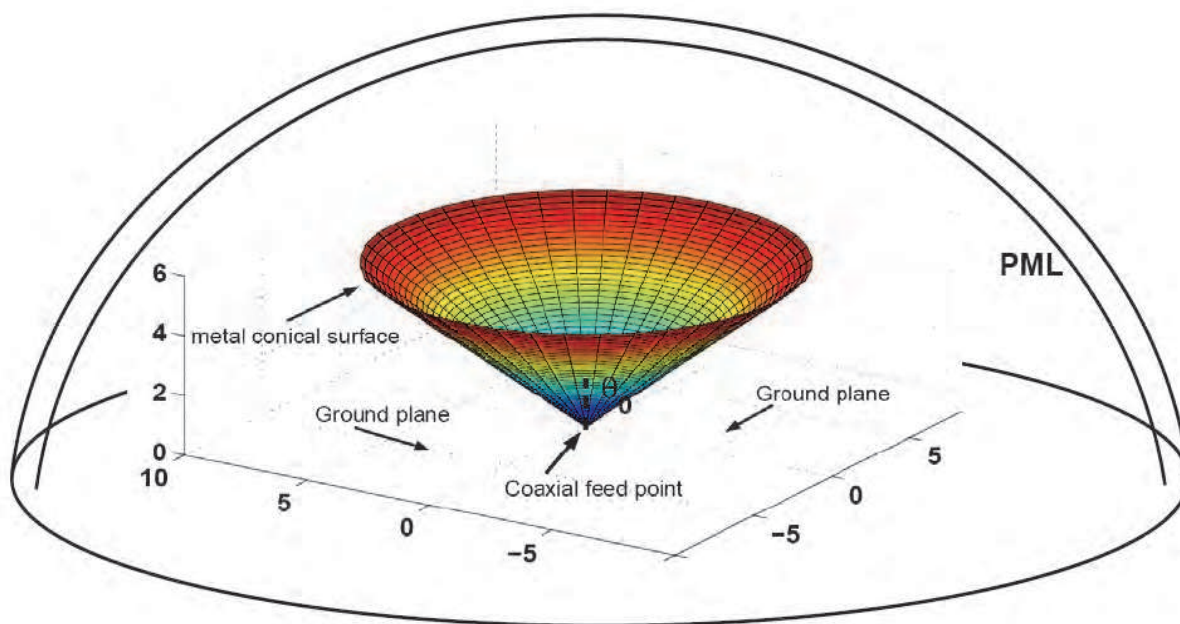


Fig. 2. Spherical perfectly matched layer at the edge of the simulation space.

In order to determine a spherical PML, the following steps must be taken:

- i. Splitting of the magnetic field component H_ϕ into two sub-components $H_{\phi r}$ and $H_{\phi\theta}$ in the coupled Maxwell equations, as follows:

$$\frac{\partial H_{\phi\theta}}{\partial t} = \frac{1}{\mu} \left[-\sigma_\theta^* H_{\phi\theta} + \frac{1}{r \sin \theta} \frac{\partial (E_r \sin \theta)}{\partial \theta} \right] \quad (12)$$

$$\frac{\partial H_{\phi r}}{\partial t} = -\frac{1}{\mu} \left[\sigma_r^* H_{\phi r} + \frac{1}{r} \frac{\partial (r \cdot E_\theta)}{\partial r} \right] \quad (13)$$

$$\frac{\partial E_r}{\partial t} = \frac{1}{\varepsilon} \left[-\sigma_\theta E_r + \frac{1}{r \sin \theta} \frac{\partial ((H_{\phi r} + H_{\phi\theta}) \sin \theta)}{\partial \theta} \right] \quad (14)$$

$$\frac{\partial E_\theta}{\partial t} = -\frac{1}{\varepsilon} \left[\sigma_r E_\theta + \frac{1}{r} \frac{\partial (r (H_{\phi r} + H_{\phi\theta}))}{\partial r} \right] \quad (15)$$

- ii. Create spherical FDTD equations from the above revised Maxwell equations:

$$H_{\phi\theta}^{n+\frac{1}{2}}(i, j) = D_{a\theta}(i) H_{\phi\theta}^{n-\frac{1}{2}}(i, j) + \frac{D_{b\theta}(i)}{(i+1/2)\Delta\theta} \cdot \left[\frac{\sin((j+1)\Delta\theta)}{\sin(j\Delta\theta)} E_r^n(i, j+1) - E_r^n(i, j) \right] \quad (16)$$

$$H_{\phi r}^{n+\frac{1}{2}}(i, j) = D_{ar}(i) H_{\phi r}^{n-\frac{1}{2}}(i, j) - D_{br}(i) \left[\left(\frac{i+1}{i} \right) E_\theta^n(i+1, j) - E_\theta^n(i, j) \right] \quad (17)$$

$$E_r^{n+1}(i, j) = C_{a\theta}(i) E_r^n(i, j) + \frac{C_{b\theta}(i)}{(i+1/2)\Delta\theta} \cdot \left[\frac{\sin((j+1/2)\Delta\theta)}{\sin((j-1/2)\Delta\theta)} H_{\phi}^{n+\frac{1}{2}}(i, j) - H_{\phi}^{n+\frac{1}{2}}(i, j-1) \right] \quad (18)$$

$$E_\theta^{n+1}(i, j) = C_{ar}(i) E_\theta^n(i, j) + C_{br}(i) \cdot \left[H_{\phi}^{n+\frac{1}{2}}(i-1, j) - \left(\frac{i+1/2}{i-1/2} \right) \cdot H_{\phi}^{n+\frac{1}{2}}(i, j) \right] \quad (19)$$

where

$$C_{ar} = \frac{1 - \frac{\sigma_r \Delta t}{2\varepsilon}}{1 + \frac{\sigma_r \Delta t}{2\varepsilon}}, \quad C_{br} = \frac{\frac{\Delta t}{\varepsilon \Delta r}}{1 + \frac{\sigma_r \Delta t}{2\varepsilon}} \quad (20)$$

$$D_{ar} = \frac{1 - \frac{\sigma_r^* \Delta t}{2\mu}}{1 + \frac{\sigma_r^* \Delta t}{2\mu}}, \quad D_{br} = \frac{\frac{\Delta t}{\mu \Delta r}}{1 + \frac{\sigma_r^* \Delta t}{2\mu}} \quad (21)$$

$$C_{a\theta} = \frac{1 - \frac{\sigma_\theta \Delta t}{2\varepsilon}}{1 + \frac{\sigma_\theta \Delta t}{2\varepsilon}}, \quad C_{b\theta} = \frac{\frac{\Delta t}{\varepsilon \Delta \theta}}{1 + \frac{\sigma_\theta \Delta t}{2\varepsilon}} \quad (22)$$

$$D_{a\theta} = \frac{1 - \frac{\sigma_\theta^* \Delta t}{2\mu}}{1 + \frac{\sigma_\theta^* \Delta t}{2\mu}}, \quad D_{b\theta} = \frac{\frac{\Delta t}{\mu \Delta \theta}}{1 + \frac{\sigma_\theta^* \Delta t}{2\mu}} \quad (23)$$

and $H_\phi = H_{\phi r} + H_{\phi \theta}$ in the last two equations.

iii. for a given number N of PMLs, calculation of free-space conductivities, σ_0 and σ_0^* , the final conductivities σ_N and σ_N^* and the conductivity profile of each PML.

According to (Berenger, 1996), for a desired conductivity profile $\sigma(r)$ of thickness δ , the reflection factor at normal incidence $R(0)$ is given by:

$$R(0) = \exp\left(-\frac{2}{\varepsilon c} \int_0^\delta \sigma(r) dr\right) \quad (24)$$

and consequently, the reflection factor for a wave at arbitrary incidence, θ , is

$$R(\theta) = R(0)^{\cos\theta} \quad (25)$$

Assuming a parabolic conductivity profile and extending the results of (Berenger, 1996) for spherical PMLs, we obtain the following equations for the desired conductivities:

a) free space conductivity:

$$\sigma_0 = -\frac{\varepsilon_0 c \ln(R(0))}{2^4 \Delta r N_{PML}^3} \quad (26)$$

b) conductivity of each layer (i):

$$\sigma(i) = \sigma_{\max} \left(\frac{i}{\delta}\right)^2, \quad \sigma_{\max} = 24\sigma_0 N_{PML} \quad (27)$$

The correct conductivity profile is calculated automatically in our code for any desired reflection factor and number of perfectly matched layers.

2.2.3 Resistive voltage source model

Antennas modelled using FDTD are often excited by a “hard” voltage source in which the internal source resistance is zero. However, a “hard” voltage source generates non-physical reflections. To avoid such problems, the base of the antenna is driven by a voltage signal $V_s(t)$ with internal resistance R_s through a coaxial line with inner and outer conductor’s diameters a and b respectively. Fig. 3 illustrates the equivalent circuit for a voltage source which includes an internal source resistance R_s .

The electric driving field E_θ , resulting from the input voltage, is given by (Liu, 1999).

$$E_\theta^n(i, j) = -\frac{V_s(t) - I_{in}(t)R_s}{b \sin(\theta) \ln(b/a)} \quad (28)$$

where

$$I_{in}(t) = (2\pi r \sin \theta) H_{\phi}(r, \theta, t) \quad (29)$$

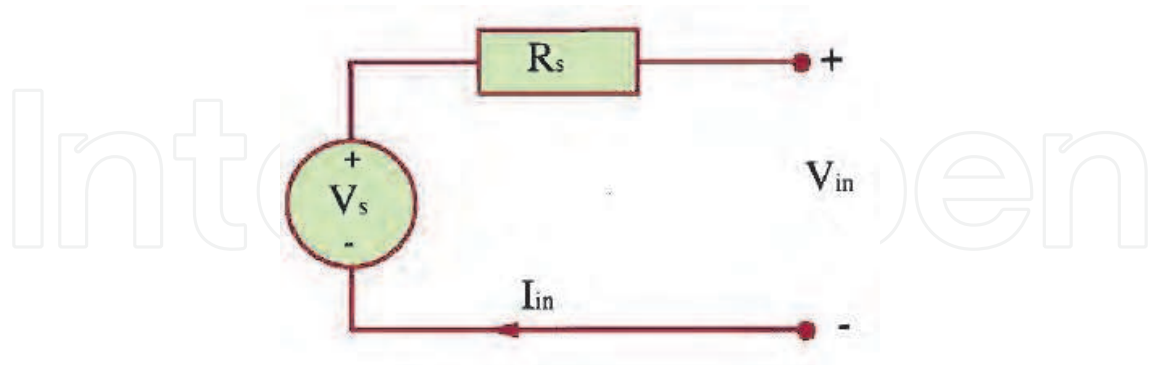


Fig. 3. Equivalent circuit of the FDTD input source.

A voltage source that corresponds to electric field of Eq. (28) can be generated in a certain mesh location $(i\Delta r, j\Delta\theta)$ within the source region and, therefore, the electric field in the source region can be written in FDTD form as

$$E_{\theta}^n(i, j) = -\frac{V_s(n\Delta t) - R_s I_{in}^{n-1/2}(i, j)}{b \cdot \sin(j\Delta\theta) \ln(b/a)} \quad (30)$$

$$I_{in}^{n-1/2}(i, j) = 2\pi(i\Delta r) \sin((j+1/2)\Delta\theta) \cdot H_{\phi}^{n-1/2}(i+1/2, j+1/2) \quad (31)$$

The above field is a spherical source extending from the inner conductor of the coaxial line to the outer conductor. Consequently, as the voltage $V_s(t)$ steps forward in time, it drives the base of the conical antenna with the above spherical field. Then, the antenna radiates the resulting wave following the time evolution described by Eq. (6)-(8).

2.3 Antenna characteristics

There are general factors determining the antenna performance for UWB applications (Stuzman & Thiele, 1997). Those are input matching represented by the input impedance, Voltage Standing Wave Ratio (VSWR) and Return Loss, frequency dependence of the maximum gain, radiation pattern determining the available beam angle for distortionless wave received from the transmitter, as well as, waveform fidelity which describes the distortion of radiated impulses. All the necessary frequency domain parameters can be calculated from the time domain parameters using a Fast Fourier Transformation code in MATLAB.

The input impedance of the antenna Z_{in} is calculated in the center of feeding line over a range of frequencies. It is determined from the ratio of the Fourier transform of the voltage wave and that of the input current wave

$$Z_{in}(f) = \frac{V_{in}(f)}{I_{in}(f)} \exp(-j\pi f \Delta t) \quad (32)$$

where the exponential term accounts for the half-time step difference between the electric and magnetic field computation.

The results of input impedance are then used to obtain the return loss characteristics of the antenna. Thus, the Return Loss S_{11} (dB) of the antenna is given by

$$S_{11}(dB) = 20 \log |\Gamma(f)| \quad (33)$$

where

$$\Gamma(f) = \frac{Z_{in}(f) - Z_{line}}{Z_{in}(f) + Z_{line}} \quad (34)$$

is the frequency dependent reflection coefficient. From the calculated reflection coefficient, the VSWR can be calculated as follows:

$$VSWR = \frac{1 + |\Gamma(f)|}{1 - |\Gamma(f)|} \quad (35)$$

The bandwidth of the antenna is the frequency range corresponding to a reflection coefficient of the antenna less than or equal to $1/3$ that leads to $VSWR \leq 2$.

To calculate the conical antenna gain, the far electric field in the desired direction must be determined as a function of frequency. Since the electric far-field is computed so that the $1/r$ amplitude factor and the propagation delay are suppressed, the antenna gain relative to a lossless isotropic antenna in θ_m - direction is given by

$$G(f, \theta_m) = \frac{1}{2\eta} \frac{|E(f, \theta_m)|^2}{P_{in} / 4\pi} \quad (36)$$

where $E(f, \theta_m)$ is the peak value of the Fourier transform of the pulsed far field radiated in the θ_m -direction, η the characteristic space impedance and P_{in} the steady-state input power at each frequency given by

$$P_{in}(f) = \frac{1}{2} \text{Re} [V_{in}(f) I_{in}^*(f)] \quad (37)$$

Directivity curves can be also computed. Directivity of an antenna is defined as the ratio of the radiation intensity in a given direction from the antenna to the radiation intensity averaged over all directions. The directivity in θ_m -direction is given by the ratio of the integral of Poynting vector with the value of electric field $E(f, \theta_m)$ to the actual value of the integral:

$$D(f, \theta_m) = \frac{2|E(f, \theta_m)|^2}{\int_0^\pi E^*(f, \theta) E(f, \theta) \sin \theta d\theta} \quad (38)$$

3. Simulation of the conical antenna characteristics

Parametric studies concerning both time domain and frequency domain characteristics of the dielectric covered conical antenna were performed using the above described spherical-coordinate FDTD algorithm implemented in MATLAB. A flowchart of the FDTD algorithm is given in Fig.4.

The FDTD cell dimensions are $\Delta r=3$ mm and $\Delta\theta=1^\circ$. The antenna sits on top of a perfectly conducting ground plane that extends 360° in all directions for a distance of $R_m=10\ell$. Just before the maximum radial distance R_m is reached, the simulation space is terminated by a PML section of thickness $20\Delta r$. The maximum reflection coefficient at normal incidence is chosen to be $R(0) = 10^{-14}$. The time step is taken $\Delta t=0.2$ psec, sufficient to satisfy Courant's criterion. An UWB Gaussian pulse (FWHM = 64 psec) modulated by a continuous sine wave carrier of frequency f_c is used in our simulations, that is,

$$V_s(t) = V_m \exp\left(-\frac{(t-t_0)^2}{\tau^2}\right) \sin(2\pi f_c(t-t_0)) \quad (39)$$

where $\tau = 64$ psec, $t_0 = 4 \times \tau$, $f_c = 6.5$ GHz and $V_m = 0.1$ V. The UWB excitation pulse driving the conical antenna is depicted in Fig.5.

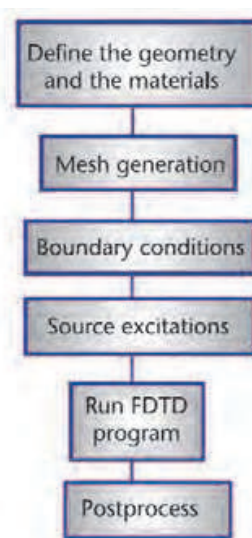


Fig. 4. Flowchart of the FDTD algorithm.

To verify the FDTD steady-state calculations, time-domain fields are transformed to the frequency domain by a Fast Fourier Transform routine. The MATLAB code was run for a wide range of different antenna's parameters combinations in an effort to find the antenna with the best match to a $50\ \Omega$ SMA-connector. FDTD has the ability to get the frequency response in one run. Accurate simulations require $2^{14} = 16384$ time steps to achieve a complete decay of the fields in the structure. The code was run on a computer equipped with an AMD Athlon 64X2 Dual Core Processor at 1.9 GHz and 2 GB of RAM memory and the computing time required to obtain a result, for specific antenna's parameters, is less than 3.5 minutes.

In the following sub-sections, we present both time-domain and frequency-domain results for a spherically dielectric covered antenna with arm's length $\ell = 45$ mm ($\sim \lambda_c = c_0/f_c$), for different loading dielectrics ϵ_r and different flare angles θ_0 . In all simulations the antenna is a small cone made of copper with conductivity of 5.8×10^7 mhos/m place at the center of the simulation space. The simulations were performed in spherical coordinates and then re-mapped to Cartesian coordinates. Finally, the Fourier transforms forward and backward are the operations to switch from frequency domain to time domain, and vice versa.

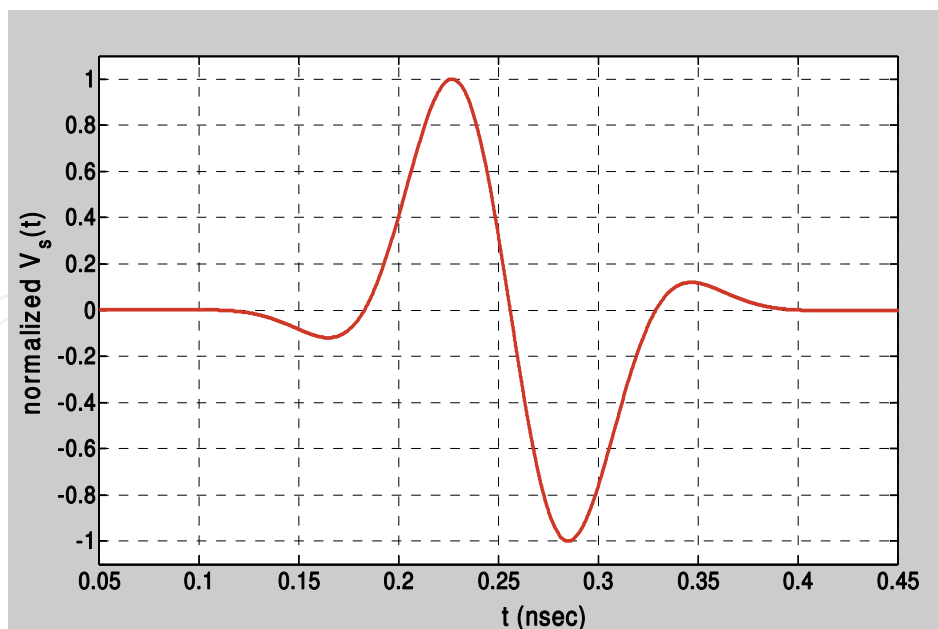


Fig. 5. Excitation UWB pulse driving the conical antenna.

3.1 Time domain characteristics

In general, our FDTD simulation provides very useful visualization of the dynamic field distributions that can help identify undesired radiation and reflection sources. Here we consider an antenna with length $\ell = 45$ mm, flare angle $\theta_0 = 47^\circ$ and dielectric cover $\epsilon_r = 3$. As you can see from Fig.6(a) the UWB pulse has started to travel out from the base of the conical antenna. The snapshot is taken after 2000 time steps or at $t = 0.4$ nsec. After 5000 time steps, i.e., at $t = 1$ nsec, the UWB pulse is propagating out of the conical antenna forming its far-field pattern shape as it is shown in Fig.6(b). The wave reflection at the dielectric - free space interface produces a wave that travels back to the antenna. The mismatch between the antenna and the feed produces a second reflection but the resulting standing wave dampens out very slowly. Figure 6(c) shows the field distribution after 9000 time steps, i.e. $t = 1.8$ nsec. The main Gaussian UWB pulse has been absorbed by the PML surrounding the simulation space but we see some small ringing arising from the imperfect mismatch between source and antenna impedances. These are not reflected from the PML region and within another 2000 steps (i.e. at $t = 2.2$ nsec) have been totally absorbed.

The main purpose of a Time-Domain study is to characterize the distortion introduced by the antenna, in terms of the angular coordinates and the excitation waveform. In narrow-band operation, it is assumed that the antenna radiates identical signals in all directions. In UWB operation, this cannot be taken for granted. The UWB antenna is excited by an incident signal whose waveform undergoes a distortion induced by the antenna. This distortion can be quantified using the correlation between the incident signal and the radiated one in certain direction, which illustrates the fidelity of the antenna in that direction (Sibille et. al., 2006). For evaluating waveform distortions caused by our dielectric covered conical antenna, we examine the degree of similarity between source pulse and received pulse waveforms in several propagation directions. Figure 7 shows that the radiated pulses, in several elevation angles θ_V , is not very different from the excitation signal and therefore, antenna's fidelity in the time-domain have been achieved. Nevertheless, a late-time ringing is observed which can be attributed to the nonlinear far-field phase over

the frequency bandwidth. The received pulses are a bit larger due to the fact that the antenna has filtered all frequencies outside the impedance bandwidth. The longer duration of the received pulses indicates lower achievable data-rates while the shape distortion can make the detection process more difficult. Proper channel models can be used to study these effects (Molisch, 2003).

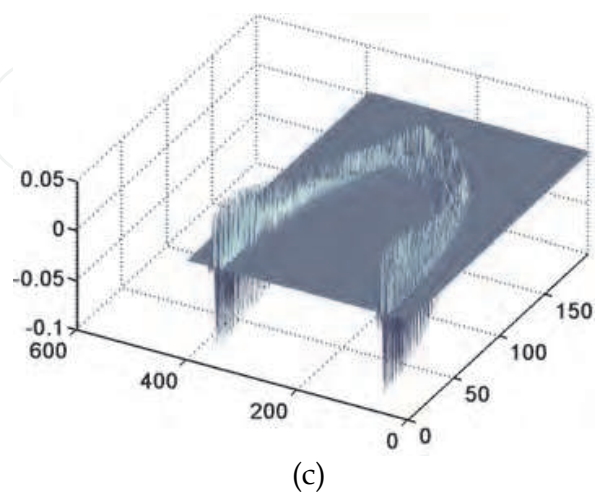
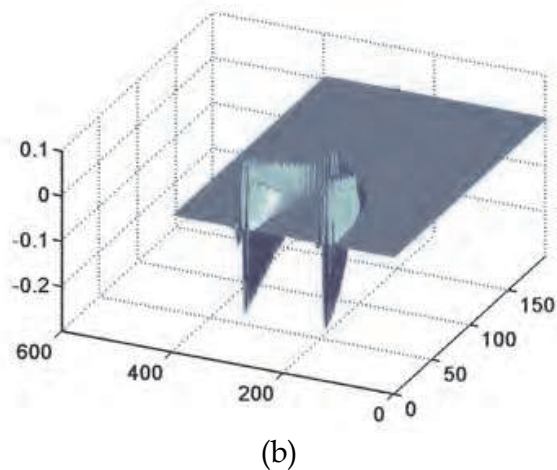
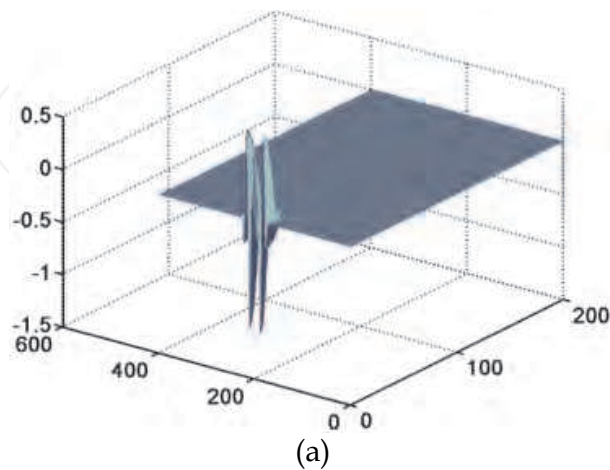


Fig. 6. FDTD simulation snapshots of the electric field strength after 2000 time steps (a), 5000 time steps (b) and 9000 time steps (c).

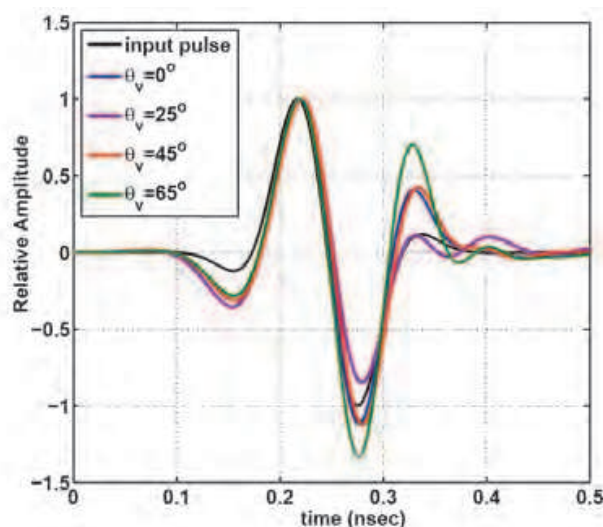


Fig. 7. Excitation and radiated pulses versus the elevation angle. It can clearly be seen that the radiated signals are elevation angle dependent.

3.2 Frequency domain characteristics

In this subsection, we present our parametric study concerning the impedance, VSWR and maximum gain of the spherically covered conical antenna varying the dielectric constant ϵ_r of the cover material or the cone flare angle.

As it is seen in Fig.9, the impedance bandwidth (VSWR < 2 or input return loss $S_{11} < -10$ dB) of the covered antenna, with dielectric of $\epsilon_r=3$, increases as the flare angle increases until reaches its maximum at $\theta_0=47^\circ$. As it is expected, the corresponding real part of input impedance (Figure 8) varies with the flare angle. It is observed that an optimum flare angle $\theta_0=47^\circ$ exists for 50Ω matched impedance in a frequency band from about 5.5 to 17 GHz. Therefore, the designed antenna can provide more than 100% impedance bandwidth.

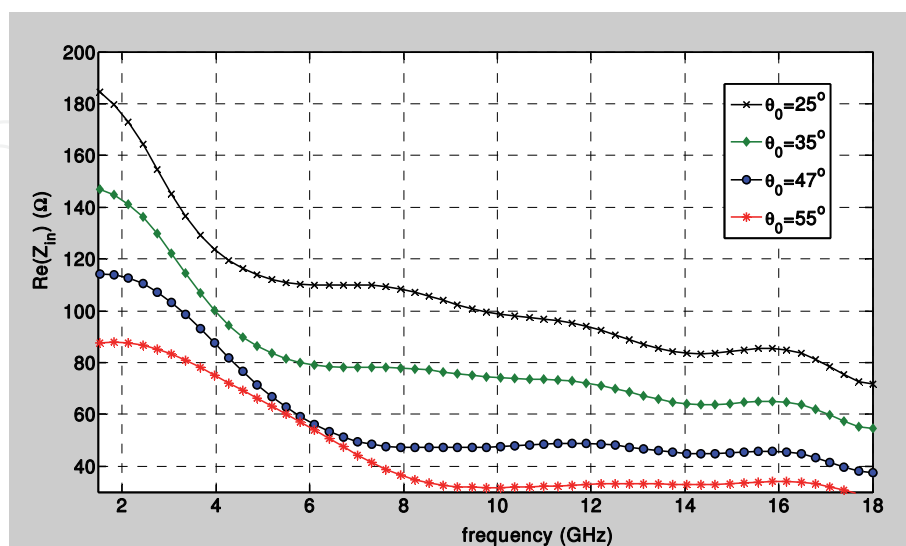


Fig. 8. Input impedance for various flare angles and $\epsilon_r=3.0$.

Figure 10, shows the evolution of maximum gain in the elevation plane (E-plane) versus frequency. Gain gradually increases with frequency from 10 dBi to about 14 dBi in the frequency range from 5.5 to 8.5 GHz and remains almost frequency independent at 14 dBi in the frequency range from 8.5 to 17 GHz.

Furthermore, the power radiation patterns in the elevation plane are calculated in the above frequency range, although for brevity, only the patterns at 4.5, 6.5, 8 and 10 GHz are shown in Fig.11. Obviously, the power radiation patterns present quasi-perfect omni-directional (monopole-like) behaviour but gradually degrade with increasing frequency. The radiation lobe enlarges downwards up to 6.5 GHz, and above 10 GHz a 'null' appears near $\theta=35^\circ$ while the beamwidth decreases slowly with frequency. These variations are attributed to the fact that the antenna's electrical size increase with frequency. It is also observed that the radiation patterns are slightly upward looking. This feature could be useful for radar sensor network applications.

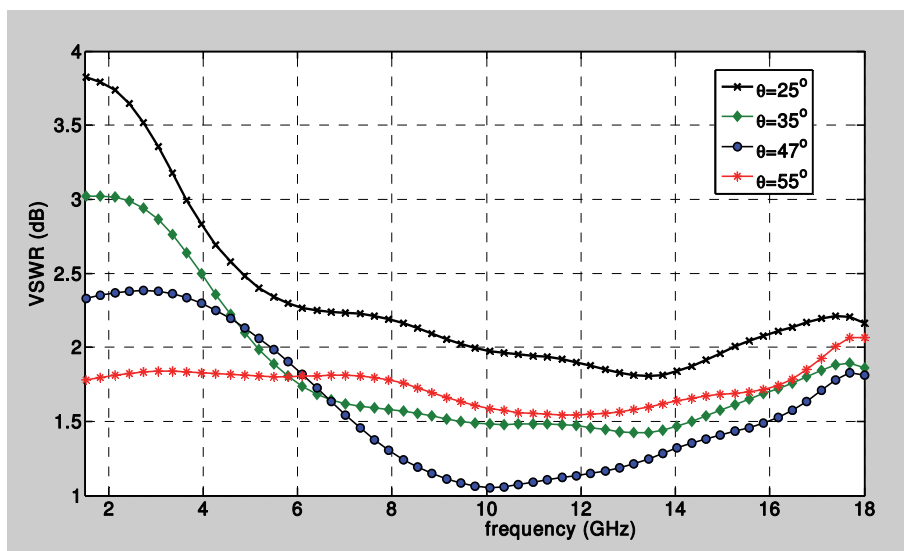


Fig. 9. Simulated VSWR for various flare angles and $\epsilon_r=3.0$.

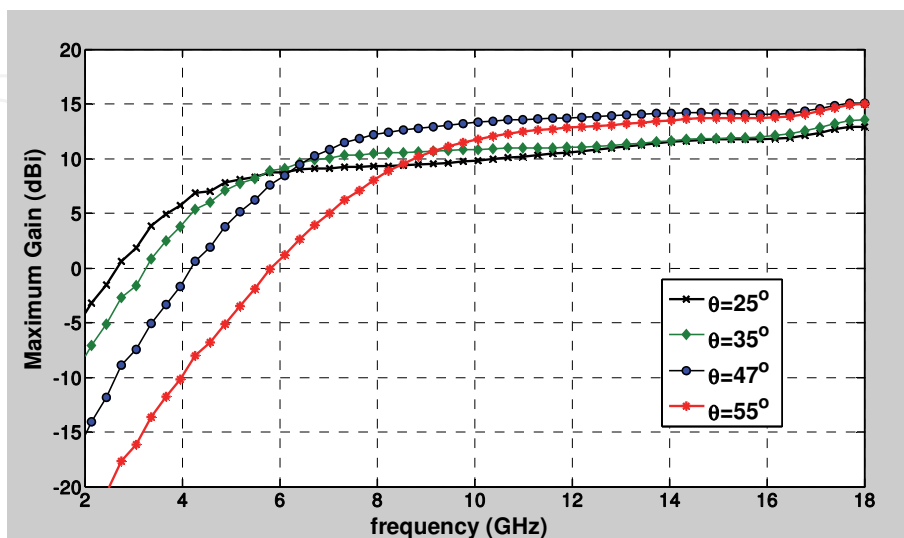


Fig. 10. Maximum gain for various flare angles and $\epsilon_r=3.0$.

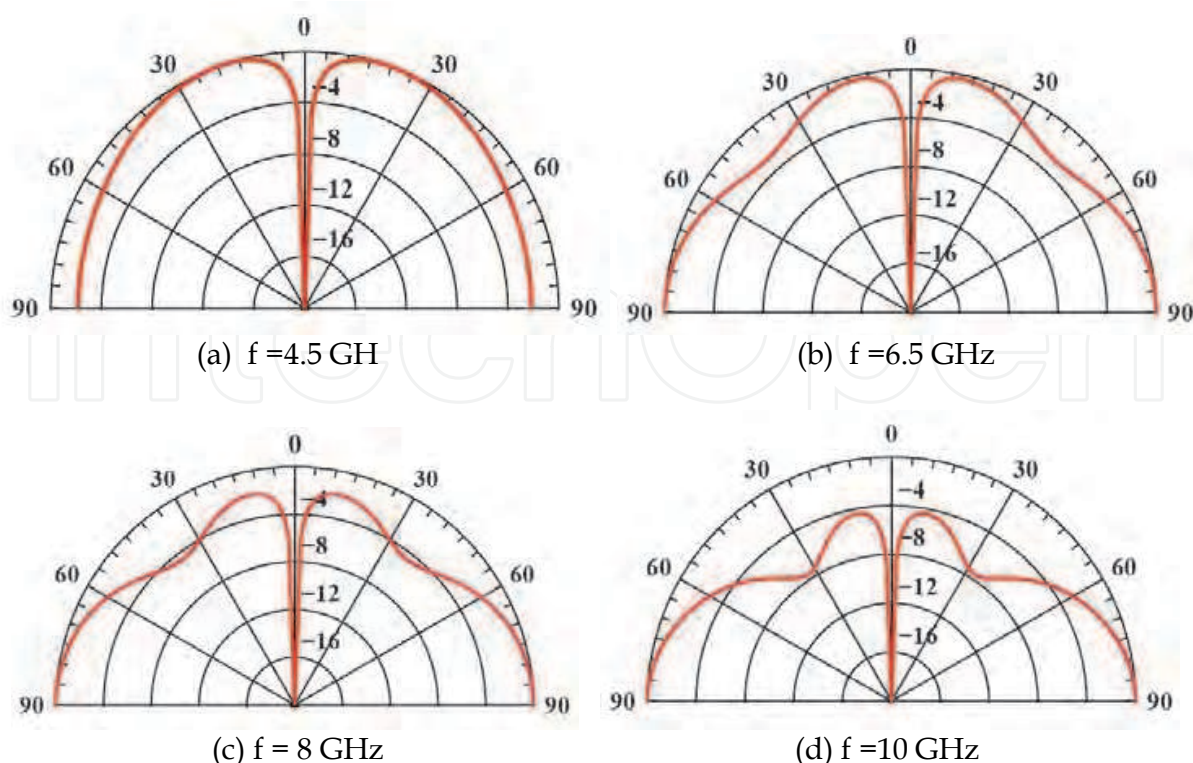


Fig. 11. Computed radiation patterns in the elevation plane at $f=4.5, 6.5, 8.0, 10.0$ GHz. The flare angle and relative dielectric constant are taken to be to $\theta=47^\circ$ and $\epsilon_r=3$, respectively.

The influence of the dielectric cover on the frequency domain characteristics of the designed antenna are investigated next. For a conical antenna with fixed flare angle $\theta_0=47^\circ$, five materials of increasing dielectric constants $\epsilon_r = 1, 2.2, 3, 4.4$ and 9.8 have been considered.

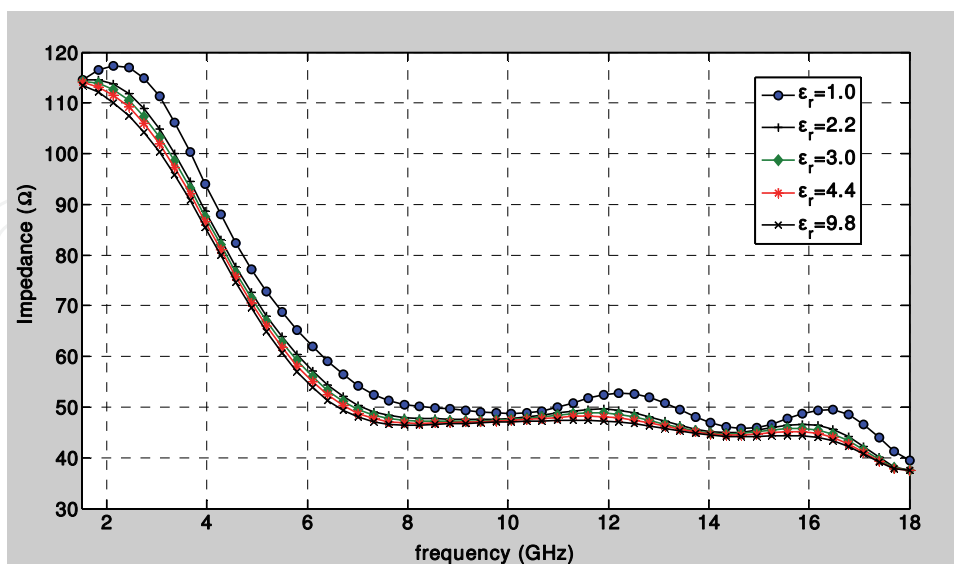


Fig. 12. Input impedance for various flare angles and $\epsilon_r=3.0$.

As it is seen in Figs.12 and 13, the ultra wide-band characteristics of the antenna are not sensitive to the variation of dielectric constant ϵ_r . Some ripples appeared in both real part of

impedance and VSWR are smoothed out when the dielectric cover is present. As it is seen, when ϵ_r is reasonably small, the antenna's input impedance remains close to a constant ($\sim 50 \Omega$) within a wide frequency band. However, because of the dielectric-air interface, the reflection and scattering at the end of the conical radiator is stronger making the antenna less matched to free space. Consequently, a wide range of dielectric materials can be used to construct the spherical cover of the antenna. Obviously, low conductivity material is preferred in order to minimize the dielectric loss. Figure 14 illustrates the frequency dependence of the maximum gain for covers of different dielectric constant. As it is seen, the maximum gain remains almost frequency independent in a wide range of frequency for all materials. However, as the dielectric constant increases, the maximum gain decreases.

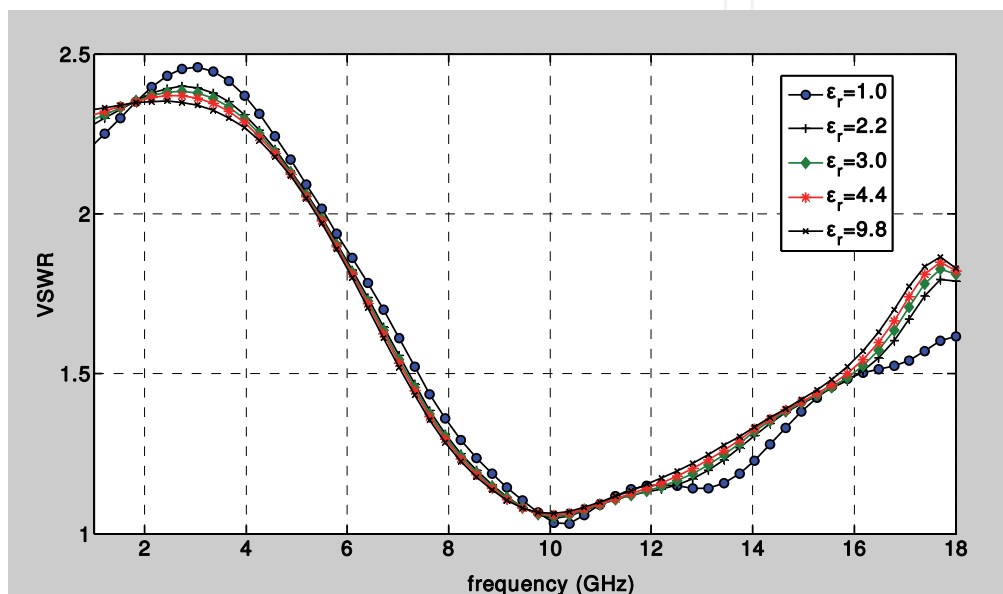


Fig. 13. Simulated VSWR for various flare angles and $\epsilon_r=3.0$.

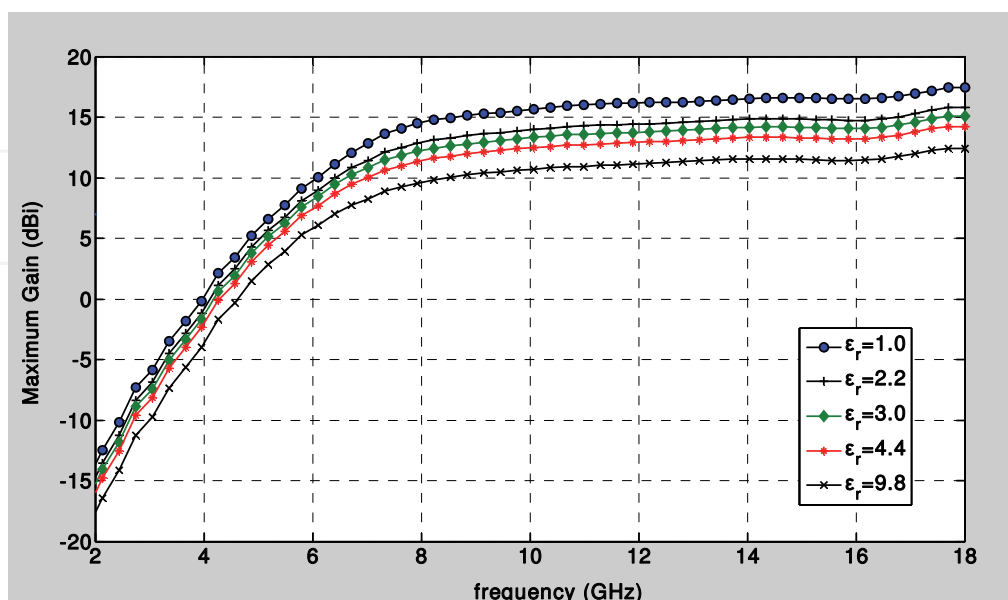


Fig. 14. Maximum gain for various flare angles and $\epsilon_r=3.0$.

4. Conclusion

In this Chapter, we present a FDTD code in spherical coordinates implemented in MATLAB in order to simulate the radiation characteristics of conical antennas. MATLAB provides an interactive environment for algorithm development, data post-processing and visualization. The spherical FDTD equations can be found using a modified Yee cell in spherical coordinates. Spherical Berenger's perfectly matched layer (PML) is applied as absorbing boundary condition where a parabolic conductivity profile in the spherical PML-region is used.

The code is used to design and simulate a conical antenna covered by a spherical dielectric structure and placed above a large ground plane. This quasi-planar antenna is mechanically stable and, relative easy to build and integrate with the planar circuits. Parametric studies lead to the optimum values of cone's arm length $\ell = 45$ mm and flare angle $\theta_0 = 47^\circ$ for 50Ω matched impedance. This design achieves an impedance bandwidth from 5.5 to 17 GHz, with stable radiation patterns over this bandwidth. The radiation patterns are monopole-like and their frequency dependence is small in the whole UWB frequency band. A time domain study has shown that the antenna distorts the excitation pulse in a moderate way.

It is observed that, the ultra wide-band characteristics of the antenna are not sensitive to the variation of dielectric constant ϵ_r of the spherical cover. Consequently, a wide range of dielectric materials can be used to construct the spherical cover of the antenna.

Our study suggests that a spherical dielectric covered conical antenna holds sufficient potential as a low-profile antenna with very wideband characteristics. A very important need is to verify more of the simulation results with experimental measurements which will be reported in a future communication.

5. Acknowledgment

The author wishes to thank his former graduate students G. Kyritsis and D. Touzloudis (now First-Lieutenants at Hellenic Air-Force) for improving and testing the first version of FDTD-code as well as some post-processing MATLAB-codes during their diploma thesis.

6. Appendix

```

=====
tmax=16384; % we use 2^{14} steps!
k=0; mu_0 = 4*pi*1e-7; eps_0 = 1e-9/(36*pi);
impedance_free=120*pi; c = 3e+8; zline=50;
% ===== Define the antenna dimensions =====
ant_length= 15;          % ant_length in units (dr) (mm).
ant_angle = 48;         % flare angle: 'ant_angle'Add (+1)for Matlab
e_rel=3.0;              % relative dielectric constant of substrate
tan_loss=0.0009d0;     % tangent loss of dielectric substrate
sub_length=ant_length; % defines dielectric substrate length
e_sub=e_rel*eps_0;
impedance_medium=impedance_free/sqrt(e_rel);
radial_view=121; % give the position (r,theta) to view the far-fields
theta_view=46;
% ===== Definitions and Constants =====
dr = 0.003;           % radial step

```

```

dth = 1.0*pi/180;      % angular step in radians
dt = 0.2e-12;         % time step in sec
tsample=0.2e-12;
radial_max =201;      % simulation space radius
theta_max = 91;      % simulation space angle
b = 0.006;           % coaxial feed-line outer radius
a = 0.003;           % coaxial feed-line inner radius
fc = 6.5e+9;         % central frequency of the spectrum
% Define the parameters of the Gaussian sine-modulated driving pulse.
td = 64e-12; t0 = 4*td; once = 0; Vmax = 0.1; Rs = 50; Zin = 0;
R0 = 1e-14;          % select the desired zero-angle reflection.
Npml = 20;           % select number of PML layers
sigma_space = - eps_0*c*log(R0)/16*dr*Npml^3;% free space conductivity
sigmaM_space = mu_0*sigma_space/eps_0;      % impedance matching condition
% calculate final conductivity for parabolic profile
sigmaPML(Npml) = 24*sigma_space*Npml^2;
sigmaMPML(Npml) = mu_0*sigmaPML(Npml)/eps_0;
for I=1:(Npml-1)
sigmaPML(I) = sigmaPML(Npml)*(I/Npml)^2;
sigmaMPML(I) = mu_0*sigmaPML(I)/eps_0;
end
for I = 1:Npml %Initialize the PML domain for magnetic field
    for J=1:theta_max
        Hpr(I,J) = 0;
        Hpt(I,J) = 0;
    end
end
% ===== Set up the conducting antenna surface =====
sigma_cu = 5.8d+7; % conductivity of Cu:5.8e+7 mhos/m
sigmaM_cu = mu_0*sigma_cu/eps_0;
sigma_epsilon = 2.d0*pi*fc*e_sub*tan_loss; %dielectric substrate losses
sigmaM_epsilon = mu_0*sigma_epsilon/e_sub;
for I =1:radial_max
for J= 1:theta_max
    if (J==ant_angle)
        if (I <= ant_length)
            sigma(I,J) = sigma_cu;
            sigmaM(I,J) = sigmaM_cu;
        elseif (I < radial_max-Npml+1)
            sigma(I,J) = sigma_space;
            sigmaM(I,J) = sigmaM_space;
        else
sigma(I,J) = sigmaPML(I + Npml - radial_max);
sigmaM(I,J) = sigmaMPML(I + Npml - radial_max);
        end
    elseif (I < ant_length)
        if (J < ant_angle)
            sigma(I,J) = sigma_space;
            sigmaM(I,J) = sigmaM_space;
        else
            sigma(I,J) = sigma_space;
            sigmaM(I,J) = sigmaM_space;
        end
    end
else
if (I< radial_max-Npml+1)
    sigma(I,J) = sigma_space;
    sigmaM(I,J) = sigmaM_space;
end
end

```

```

else
sigma(I,J) = sigmaPML(I + Npml - radial_max);
sigmaM(I,J) = sigmaMPML(I + Npml - radial_max);
end
end
if ((I <=sub_length) & (J > ant_angle) & (J< (theta_max-1)))
sigma(I,J)= sigma_epsilon;
sigmaM(I,J)= sigmaM_epsilon;
end
end
for I = 1:radial_max %initialize, zero the fields for all free nodes
for J= 1:theta_max
if ((I >= ant_length) | (J >= ant_angle))
Er(I,J) = 0; Et(I,J) = 0; Hp(I,J) = 0;
end
end
end
g1 = dt/(2*mu_0); g2 = dt/(2*eps_0);
g3 = dt/(dr*eps_0); g4 = dt/(dr*mu_0);
I_factor = 2*pi*b;
V_factor = (log(sin(ant_angle*pi/180))-log(1-cos(ant_angle*pi/180)))/log(2);
%===== Begin of time iterations =====
t = 0;
fid=fopen('Etime.dat', 'wt');
while (t < (tmax*dt))
t = t + 0.5*dt; % For the first half time-step, update the H-field.
for I = 3:(radial_max-Npml)
for J = 2:(theta_max-1)
if ((I >= ant_length) | (J >= ant_angle))
g5 = sin(J*dth)/sin((J-1)*dth);
Da = (1-sigmaM(I,J)*g1)/(1+sigmaM(I,J)*g1);
Db = g4/(1+sigmaM(I,J)*g1);
ER1 = (g5*Er(I,J+1)-Er(I,J))/((I-1/2)*dth);
ET1 = (I/(I-1))*Et(I+1,J) - Et(I,J);
Hp(I,J) = Da*Hp(I,J) + Db*(ER1 - ET1);
end
end
end
J = theta_max; % H-field at the ground plane
for I = 3:(radial_max-Npml)
Da = (1-sigmaM(I,J)*g1)/(1+sigmaM(I,J)*g1);
Db = g4/(1+sigmaM(I,J)*g1);
ET1 = (I/(I-1))*Et(I+1,J) - Et(I,J);
Hp(I,J) = Da*Hp(I,J) - Db*ET1;
end
for I = ant_length:(radial_max-Npml)
Hp(I,1) = Hp(I,2); % H-field along the line of symmetry
end
layer = 1; % Update the H-field in the PML region
for I = (radial_max-Npml+1):radial_max
Dar = (1-sigmaMPML(layer)*g1)/(1+sigmaMPML(layer)*g1);
Dbr = g4/(1+sigmaMPML(layer)*g1);
Dat = Dar; Dbt = Dbr;
for J = 2:(theta_max-1)
g5 = sin(J*dth)/sin((J-1)*dth);
ER1 = (g5*Er(I,J+1)-Er(I,J))/((I-1/2)*dth);

```

```

if(I == radial_max)
ET1 = 0;
else
ET1 = (I/(I-1))*Et(I+1,J) - Et(I,J);
end
Hpr(layer,J) = Dar*Hpr(layer,J) - Dbr*ET1;
Hpt(layer,J) = Dat*Hpt(layer,J) + Dbt*ER1;
Hp(I,J) = Hpr(layer,J) + Hpt(layer,J);
end
layer = layer + 1;
end
J = theta_max; % Update H-field in the PML along the ground plane
layer = 1;
for I = (radial_max-Npml+1):radial_max
Dar = (1-sigmaMPML(layer)*g1)/(1+sigmaMPML(layer)*g1);
Dbr = g4/(1+sigmaMPML(layer)*g1);
Dat = Dar;
if(I == radial_max)
ET1 = 0;
else
ET1 = (I/(I-1))*Et(I+1,J) - Et(I,J);
end
Hpr(layer,J) = Dar*Hpr(layer,J) - Dbr*ET1;
Hpt(layer,J) = Dat*Hpt(layer,J);
Hp(I,J) = Hpr(layer,J) + Hpt(layer,J);
layer = layer + 1;
end
t = t + 0.5*dt; % For the second half time-step, update the E-fields.
Vsource= Vmax*exp(-((t-t0)/td)^2)*sin(2*pi*fc*(t-t0));
Vin = 0; Iins = 0;
for J = ant_angle:theta_max
Iin = I_factor*sin((J-1/2)*dth)*Hp(3,J);
Vdrv = Vsource- Rs*Iin;
if ((t >= tsample) & (J > ant_angle))
Vin = Vin + b*Et(3,J)*dth;
Iins = Iins + Iin;
if(J == (theta_max-1))
Iins = Iins/(theta_max - ant_angle -1);
exVin = Vin; exIin = Iin;
end
end
Et(3,J) = Vdrv*(1/(b*log(2)))/sin((J-1/2)*dth);
end
k=k+1;
piVin(k)=Vin;
piIin(k)=Iin;
for I = 4:(radial_max-Npml) % Step E-fields for free nodes
for J = 2:(theta_max-1)
if ((I >= ant_length) | (J >= ant_angle))
g6 = sin((J-1/2)*dth)/sin((J-3/2)*dth);
Ca = (1 - g2*sigma(I,J))/(1 + g2*sigma(I,J));
Cb = g3/(1 + g2*sigma(I,J));
HPHI1 = (g6*Hp(I,J) - Hp(I,J-1))/(I-1/2)*dth;
HPHI2 = Hp(I-1,J) - ((I-1/2)/(I-3/2))*Hp(I,J);
Er(I,J) = Ca*Er(I,J) + Cb*HPHI1;
Et(I,J) = Ca*Et(I,J) + Cb*HPHI2;
end

```

```

end
end
% ===== Introduction of spherical dielectric cover =====
for I = 4:sub_length
    for J = ant_angle:theta_max-1
        g6 = sin((J-0.5)*dth)/sin((J-1.5)*dth);
        g2_sub = 1/(1*e_sub/eps_0);
        g3_sub = 1/(1*e_sub/eps_0);
        Ca = (1 - g2_sub*sigma(I,J))/(1+ g2_sub*sigma(I,J));
        Cb = g3_sub/(1 + g2_sub*sigma(I,J));
        HPHI1 = (g6*Hp(I,J)- Hp(I,J-1))/((I-0.5)*dth);
        HPHI2 = Hp(I-1,J)-((I-0.5)/(I-1.5))*Hp(I,J);
        Er(I,J) = Ca*Er(I,J) + Cb*HPHI1;
        Et(I,J) = Ca*Et(I,J) + Cb*HPHI2;
    end
end
J = theta_max;E % Compute the fields at the ground plane
for I = 4:(radial_max-Npml)
    Ca = (1 - g2*sigma(I,J))/(1+ g2*sigma(I,J));
    Cb = g3/(1 + g2*sigma(I,J));
    HPHI2 = Hp(I-1,J) - ((I-1/2)/(I-3/2))*Hp(I,J);
    Er(I,J) = 0;
    Et(I,J) = Ca*Et(I,J) + Cb*HPHI2;
end
J = theta_max; % Compute the E-fields for the substrate domain
for I = 4:sub_length
    g2_sub = 1/(1*e_sub/eps_0);
    g3_sub = 1/(1*e_sub/eps_0);
    Ca = (1 - g2_sub*sigma(I,J))/(1+ g2_sub*sigma(I,J));
    Cb = g3_sub/(1 + g2_sub*sigma(I,J));
    HPHI2 = Hp(I-1,J) - ((I-1/2)/(I-3/2))*Hp(I,J);
    Er(I,J) = 0;
    Et(I,J) = Ca*Et(I,J) + Cb*HPHI2;
end
for I = ant_length:(radial_max-Npml) %E-field along line of symmetry
    Ca = (1 - g2*sigma(I,1))/(1 + g2*sigma(I,1));
    Cb = g3/(1+g2*sigma(I,1));
    HPHI1 = (Hp(I,2) - Hp(I,1))/((I-1/2)*dth);
    Er(I,1) = Ca*Er(I,1) + Cb*HPHI1;
    Et(I,1) = 0;
end
layer = 1; % Update the E-fields in the PML region
for I = (radial_max-Npml+1):radial_max
    for J = 2:(theta_max-1)
        g6 = sin((J-1/2)*dth)/sin((J-3/2)*dth);
        Car = (1 - g2*sigmaPML(layer))/(1 + g2*sigmaPML(layer));
        Cbr = g3/(1 + g2*sigmaPML(layer));
        Cat = Car; Cbt = Cbr;
        HPHI1 = (g6*Hp(I,J) - Hp(I,J-1))/((I-1/2)*dth);
        HPHI2 = (Hp(I-1,J) - ((I-1/2)/(I-3/2))*Hp(I,J));
        Er(I,J) = Cat*Er(I,J) + Cbt*HPHI1;
        Et(I,J) = Car*Et(I,J) + Cbr*HPHI2;
    end
end
layer = layer + 1;
end
layer = 1; %E-field in the PML region at the ground plane
J = theta_max;

```

```

for I = (radial_max-Npml+1):radial_max
Car = (1 - g2*sigmaPML(layer))/(1 + g2*sigmaPML(layer));
Cbr = g3/(1 + g2*sigmaPML(layer));
HPHI2 = (Hp(I-1,J) - ((I-1/2)/(I-3/2))*Hp(I,J));
Er(I,J) = 0; Et(I,J) = Car*Et(I,J) + Cbr*HPHI2;
layer = layer + 1;
end
Etheta(k)=Et(radial_view,theta_view);
Radial_view=151; tt=t/1e-12;
for sJ=1:theta_max-1
    EthetaT(sJ,k)=Et(radial_view,sJ);
end
end
fclose(fid);
table=[tt; Et(radial_view, theta_view)];
%===== Spherical to rectangular coordinates transformation =====
for I=1:radial_max
    for J=1:theta_max-1
        x= radial_max +round((I*sin((J-1)*dth));
        x2 = (2*radial_max+1) - x; y = 1 + round((I*cos((J-1)*dth));
        Ecart(x,y) = Et(I,J); Ecart(x2,y) = Et(I,J);
    end
end
for I=1:(2*radial_max-1)
    for J = 1:radial_max
        EcartNew(I,J) = Ecart(I,J);
    end
end
Imin = 2; Imax = 2*radial_max - 2; Jmin = 2; Jmax = radial_max-1;
for I = Imin:Imax
    for J = Jmin:Jmax
        if ((Ecart(I,J)=0)&(radial_max*cos((I-radial_max)*dth*91/151)+25>= J))
            ItempLo = I-1; ItempHi = I+1;
            while ((Ecart(ItempLo,J) == 0) & (ItempLo > 1))
                ItempLo = ItempLo-1;
            end
            while ((Ecart(ItempHi,J) == 0) & (ItempHi < 2*radial_max -1))
                ItempHi = ItempHi + 1;
            end
            M = Ecart(ItempLo,J); N = Ecart(ItempHi,J);
            if(M == 0)
                temp1 = N;
            elseif(N == 0)
                temp1 = M;
            else
                temp1 = sign(M+N)*sqrt(abs(M*N));
            end
            JtempLo = J-1; JtempHi = J+1;
            while ((Ecart(I,JtempLo)= 0) & (JtempLo > 1))
                JtempLo = JtempLo-1;
            end
            while ((Ecart(I,JtempHi)= 0) & (JtempHi < radial_max))
                JtempHi = JtempHi + 1;
            end
            M = Ecart(I,JtempLo); N = Ecart(I,JtempHi);
            if(M == 0)
                temp2 = N;

```

```

        elseif(N == 0)
            temp2 = M;
        else
            temp2 = sign(M+N)*sqrt(abs(M*N));
        end
        if (temp1==0)
            EcartNew(I,J) = temp2;
        elseif(temp2 == 0)
            EcartNew(I,J) = temp1;
        else
            EcartNew(I,J) = sign(temp1+temp2)*sqrt(abs(temp1*temp2));
        end
    end
end
EcartNew(1,radial_max)=1.0; EcartNew(2,radial_max)= -1.0;
end
%===== 3D time evolution of E-field =====
I=1:2*radial_max-1; J=1:radial_max;
x(I) = I; y(J) = J;
surf1(y(J), x(I), EcartNew(I,J))
xlabel('Y-axis cm'), ylabel('X-axis cm')
zlabel('Etheta V/m')
shading interp; colormap bone
%===== Frequency-Domain Analysis =====
t_val=0.2e-12:0.2e-12:0.2e-12*tmax;
dt = t_val(2) - t_val(1); t0 = t_val(1); V_val=piVin; I_val=piIin;
iplot = 1; ipad = 0; omega_plot_max =2*pi*10e9; omin=2; omax=61;
central_f=14; % omega (14) corresponds to frequency 6.5 GHz!
Vft_power,Vft,omega,iflag] =
get_Fourier_transform(dt,t0,V_val,iplot,ipad,omega_plot_max);%Call FFT
iflag=0; N=length(Vft);
[Ift_power,Ift,omega,iflag] = ...
get_Fourier_transform(dt,t0,I_val,iplot,ipad,omega_plot_max);
Z_FT=complex(zeros(1,N),zeros(1,N)); cutoff=1e-25;
for m=1:N
    if(abs(Ift(m)< cutoff))
        Z_FT(m)=0;
    else
        Z_FT(m)=Vft(m)/Ift(m);
    end
end
end
j=1:N; Z=Z_FT(j); % Impedance Matrix
imath=sqrt(-1); phase=exp(-imath*0.5*omega*dt);
ZTR1=Vft./Ift; ZTR=ZTR1.*phase;
Re=real(ZTR); Im=imag(ZTR); Zabs=abs(ZTR);
plot(omega(omin:omax)/(2*pi*1e9),Re(omin:omax),'k-.')
xlabel('frequency (GHz)'); ylabel('Impedance (Ohms)');
GAMMA=(ZTR-Zline)/(ZTR+Zline); % Reflection coefficient
RLoss=20*log10(abs(GAMMA)); % Input Return Loss in (dB)
VSWR=(1+abs(GAMMA))/(1-abs(GAMMA)); % Voltage standing wave ratio
plot(omega(omin:omax)/(2*pi*1e9),VSWR(omin:omax),'k-.')
xlabel('frequency (GHz)'); ylabel('VSWR');
FeedPower=0.5*real(Vft.*conj(Ift)); % Input Power versus frequency
omeg=omega(central_f);
plot(omega(omin:omax)/(2*pi*1e9),RLoss(omin:omax),'k-.')
xlabel('Frequency (GHz)'); ylabel('Return Loss (dB)');

```



```

% =====Directivity & Gain =====
iflag=0; % used in the FFT-routine
for J=2:theta_max-1
    itime=1:k;
    iplot_new=0;
    Etheta_val=EthetaT(J,itime);
    EthetaJft_power,EthetaJft_omega,iflag] = ...
    get_Fourier_transform(dt,t0,Etheta_val,iplot_new,ipad,omega_plot_max);
    Gain=(2*pi/impedance_medium)*EthetaJft_power./FeedPower;
    Gain_theta(J,:)=Gain; Gain_Max(J)=max(Gain(:));
    Directivity(J,:)=EthetaJft_power;
end
J=2:theta_max-1; itime=1:k;
Gain_elevation=Gain_theta(J,itime);
    for itime=omin+1:omax;
        GMax_F(itime)=max(Gain_elevation(:,itime));
    end
plot(omega(omin:omax)/(2*pi*1e9),10*log10(GMax_F(omin:omax)),'k.')
xlabel('Frequency (GHz)'); ylabel('Maximum Gain (dBi)');
for itime=1:k;
    step=1; arg=2:(theta_max-1);
    f=Directivity(arg,itime);%Directivity as a function of  $\theta$  and time-step
    g=sin(arg.*pi/180); fun=f*g;
    table = cumtrapz(fun)*step*pi/180; % Integration over angle theta
    integral=table(theta_max-2)-table(1); intg(itime)=integral;
end
% ===== Power Radiation Pattern =====
theta_max=91; radial_max=0;
rmin=-20; rticks=10;
line_style='-';
thetal=1:theta_max-1;
FFP= Directivity(thetal,central_f);
D11=10*log10(FFP./max(FFP));
th1=[1:length(D11)]';
hpol = polar_dB(th1,D11,rmin,radial_max,rticks,line_style);
hold on;
th1=[1:length(D11)]';
hpol = polar_dB(360-th1,D11,rmin,radial_max,rticks,line_style);

```

Table 1. FDTD simulation of a dielectric covered conical uwb antenna in MATLAB.

7. References

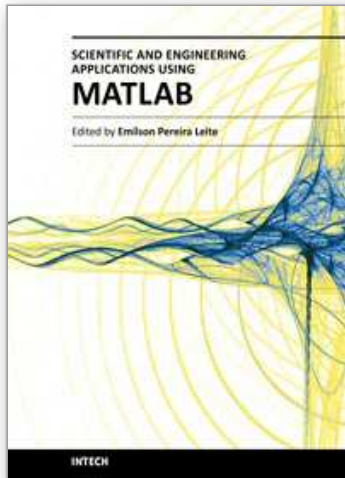
- Berenger J.P. (1996). Perfectly Matched Layer for the FDTD Solution of Wave-Structure Interaction Problems. *IEEE Transactions on Antennas & Propagation*, Vol.44, No. 1, pp. 110-117
- Brocato, R. W. (2004). *FDTD simulation tools for UWB antenna analysis*, Sandia Report, SAND2004-6577, Sandia National Laboratories.
- Fusco M. (1990). FDTD Algorithm in Curvilinear Coordinates. *IEEE Transactions on Antennas & Propagation*, 38, pp. 76-89
- Harrison C. W., Jr. & C. S. Williams, Jr. (1965). Transients in Wide-Angle Conical Antennas, *IEEE Transactions on. Antennas & Propagation*, Vol. AP-13, pp. 236-246

- Gentili G. B., Cerretelli M. and Cecchi L. (2004). Coated conical antennas for automotive application. *Journal Electromagnetic Waves & Applications*, Vol.18, No.1, pp. 85-97
- Katz, D.S., Thiele, E.T & Taflove, A. (1994). Validation and extension to three dimensions of the Berenger PML absorbing boundary condition for FDTD meshes. *IEEE Microwave & Guided Wave Letters*, Vol, 4, No.8, pp. 268 - 270
- Kliros G. S., Kyritsis G. & Touzloudis D. (2010), Dielectric-EBG covered conical antenna for UWB applications. *COMPEL: International Journal for Computation & Mathematics in Electrical and Electronic Engineering*, Vol. 29, no. 4, pp. 1134-1143
- Kliros G. S., Kyritsis G. & Touzloudis D. (2010). FDTD Analysis of a Conical Microstrip Antenna on EBG-substrate. *Journal of Applied Electromagnetism (JAE)*, Vol. 12, No.1, pp.1-8, ISSN: 1109-1606
- Liang X. & Wah M. C. Y. (2000). Low-profile broadband omni-directional monopole antenna. *Microwave & Optical Technology Letters*, Vol. 25, No. 2, pp.135-138
- Liu G. & Grimes C. (1999). Spherical-coordinate FDTD analysis of conical antennas mounted above finite ground planes. *Microwave & Optical Technology Letters*, Vol.23, pp.78-82
- Lu M., Bredow J., Jung S. & Tjuatja S. (2007). A Quasi-Planar Wide Band Conical Antenna. In: *Ultra-Wide Band Short-Pulse Electromagnetics*, Baum, C. E., Stone, A. P., Tyo, J. S. (Eds.), pp. 25-32, Springer, ISBN 978-0-387-73045-5, New York
- Ma J., Yin Y.Z., Zhou S.G. & Zhao L.Y. (2009). Design of a new wideband low-profile conical antenna. *Microwave & Optical Technology Letters*, Vol.51, No.11, pp. 2620-2623
- Maloney J. G. & Smith G. S. (1993). Optimization of a conical antenna for pulse radiation: an efficient design using resistive loading. *IEEE Transactions on Antennas & Propagation*, Vol. 41, No.7, pp.940-947
- Minin, I. (Ed.). (March 2010). *Microwave & Millimeter Wave Technologies Modern UWB antennas and equipment*, InTech, ISBN 978-953-7619-67-1, Croatia
- Molisch A.F. , Foerster J. R. & Pendergrass, M. (2003). Channel models for ultrawide-band personal area networks. *IEEE Wireless Communications*, Vol. 10, pp. 14-21
- Palud S., Colombel F., Himdi M., Le Meins C. (2008). Compact multi-octave conical antenna. *Electronics Letters*, Vol. 44, No. 11, pp 659-661
- Sandler S. & King R.W.P. (1994). Compact conical antennas for wide-band coverage. *IEEE Transactions on Antennas & Propagation*, Vol.42, No.3, pp 436-439
- Sibille A., Roblin C., Bories S. & Lepage A. C. (2006). A Channel-Based Statistical Approach to Antenna Performance in UWB Communications. *IEEE Transactions on Antennas & Propagation* Vol. 54, No. 11, pp. 3207-3215
- Stuzman W. A. & Thiele G. L. (1997). *Antenna theory and Design*, 2nd ed., John Wiley & Sons, ISBN: 0-471-02590-9, New York
- Taflove A. & Hagness S. C. (2005). *Computational electrodynamics: the finite-difference time-domain method*, 3rd ed., pp. 411-472, ISBN 978-1-58053-832-9, Artech House, Boston
- Yee K. (1996). Numerical solution of initial boundary value problems involving Maxwell's equations in isotropic media. *IEEE Transactions on Antennas and Propagation*, Vol.14, pp. 302-307
- Yu Y. K. & Li J. (2008). Analysis of electrically small size conical antennas. *Progress in Electromagnetic Research Letters*, Vol. 1, pp. 85-92

- Zhou S., Ma J., Deng J., & Liu Q. (2009). A low-profile and broadband conical antenna. *Progress in Electromagnetic Research Letter*, Vol.7, pp. 97-103
- Wiesbeck W., Adamiuk G. & Sturm C. (2009). Basic properties and design principles of UWB antennas. *Proceedings of the IEEE*, Vol. 97, No.2, pp.372-385

IntechOpen

IntechOpen



Scientific and Engineering Applications Using MATLAB

Edited by Prof. Emilson Pereira Leite

ISBN 978-953-307-659-1

Hard cover, 204 pages

Publisher InTech

Published online 01, August, 2011

Published in print edition August, 2011

The purpose of this book is to present 10 scientific and engineering works whose numerical and graphical analysis were all constructed using the power of MATLAB® tools. The first five chapters of this book show applications in seismology, meteorology and natural environment. Chapters 6 and 7 focus on modeling and simulation of Water Distribution Networks. Simulation was also applied to study wide area protection for interconnected power grids (Chapter 8) and performance of conical antennas (Chapter 9). The last chapter deals with depth positioning of underwater robot vehicles. Therefore, this book is a collection of interesting examples of where this computational package can be applied.

How to reference

In order to correctly reference this scholarly work, feel free to copy and paste the following:

George S. Kliros (2011). Simulated Performance of Conical Antennas Using Matlab-Based Finite-Difference Time Domain (FDTD) Code, Scientific and Engineering Applications Using MATLAB, Prof. Emilson Pereira Leite (Ed.), ISBN: 978-953-307-659-1, InTech, Available from: <http://www.intechopen.com/books/scientific-and-engineering-applications-using-matlab/simulated-performance-of-conical-antennas-using-matlab-based-finite-difference-time-domain-fdtd-code>

INTECH
open science | open minds

InTech Europe

University Campus STeP Ri
Slavka Krautzeka 83/A
51000 Rijeka, Croatia
Phone: +385 (51) 770 447
Fax: +385 (51) 686 166
www.intechopen.com

InTech China

Unit 405, Office Block, Hotel Equatorial Shanghai
No.65, Yan An Road (West), Shanghai, 200040, China
中国上海市延安西路65号上海国际贵都大饭店办公楼405单元
Phone: +86-21-62489820
Fax: +86-21-62489821

© 2011 The Author(s). Licensee IntechOpen. This chapter is distributed under the terms of the [Creative Commons Attribution-NonCommercial-ShareAlike-3.0 License](#), which permits use, distribution and reproduction for non-commercial purposes, provided the original is properly cited and derivative works building on this content are distributed under the same license.

IntechOpen

IntechOpen